Surface smoothing: a way back in early brain morphogenesis

Julien Lefèvre[1,2] *, Victor Intwali[3], Lucie Hertz-Pannier[4,5], Petra S. Hüppi[6], Jean-Francois Mangin[5], Jessica Dubois[7], and David Germanaud[4,5]

[1] Aix-Marseille Univ, Département d'Informatique et Interractions, Marseille, France
[2] CNRS, LSIS, UMR 7296, Marseille, France, julien.lefevre@univ-amu.fr
[3] Ecole Centrale Marseille, France
[4] UMR 663, INSERM, Université Paris Descartes, Paris, France
[5] CEA, I2BM, DSV, NeuroSpin, Gif/Yvette, France
[6] Geneva University Hospitals, Department of Pediatrics, Switzerland
[7] U992, INSERM, NeuroSpin, Gif/Yvette, France

Abstract. In this article we propose to investigate the analogy between early cortical folding process and cortical smoothing by mean curvature flow. First, we introduce a one-parameter model that is able to fit a developmental trajectory as represented in a Volume-Area plot and we propose an efficient optimization strategy for parameter estimation. Second, we validate the model on forty cortical surfaces of preterm newborns by comparing global geometrical indices and trajectories of central sulcus along developmental and simulation time.

1 Introduction

The onset and rapid extension of cortical folds between 20 and 40 weeks of human gestation has been long known from ex vivo examination and observed in vivo since the early days of MRI [10]. Recently reconstruction and segmentation techniques have allowed to study more quantitatively normal developmental

* This work is funded by the Agence Nationale de la Recherche (ANR-12-JS03-001-01, 'Modegy').

trajectories of premature newborns [6] or foetus [15, 4] as well as abnormal trajectories in diseases such as ventriculomegaly [16].

Nevertheless the normal and abnormal gyrification process is still suffering from a lack of comprehensive biological mechanisms. In this context several numerical models have been proposed recently with different underlying hypotheses such as mechanical tensions along white matter fibers [8], genetic determination of future gyri [18, 13] or tissue growth [19] that can be modulated by skull constraints [14]. However there is no real consensus on this issue and validations are often focused on a limited number of parameters.

Other approaches have modeled cortical folding process in a less biologically explicit but maybe more pragmatic way. Harmonic analysis has been proposed through spherical wavelets [20] or manifold harmonics (Laplace-Beltrami eigenfunctions) [9]. They both make an analogy between the appearance of new folds and the addition of new non-vanishing components in the spectral decomposition of surface coordinates. A related approach was found before in [2] where a scale-space of the mean curvature was used to recover the early steps of gyrogenesis and identify "sulcal roots" - putative elementary atoms of cortical folds. This last theory has been used to study the issue of cortical folding variability but to our knowledge it has never been confronted to real developmental data.

That is why this article aims at going beyond a strict visual analogy by testing in which extent some geometric flows can play backward the gyrification process. Our contributions are twofold: first we propose a 1 parameter model derived from mean curvature flow as well as an optimization procedure to fit the parameter on any brain developmental sequence. Second, we present validation tools based on global geometric indices and sulci, tested on 40 preterm newborns.

2 Methodology

2.1 Mathematical preliminaries

In the following we will consider $\mathcal{M}_0$ a compact surface of $\mathbb{R}^3$, without boundaries, which will be a left hemisphere in our applications. $\mathcal{M}_0$ can be represented

by local mappings around open sets U, $Q : U \subset \mathbb{R}^2 \to Q(U) \subset \mathcal{M}_0 \subset \mathbb{R}^3$. The surface is supposed to be smooth enough to define a normal vector $N(\mathbf{x})$, oriented from the outside to the inside and principal curvatures $\kappa_1 \geq \kappa_2$ at each point $\mathbf{x}$. The mean curvature $H(\mathbf{x})$ is given by $(\kappa_1 + \kappa_2)/2$. Thus the mean curvature flow equation can be defined by two equivalent ways :

$$\partial_t P(\mathbf{x}, t) = H(\mathbf{x}, t) N(\mathbf{x}, t) \quad (1) \qquad \partial_t P(\mathbf{x}, t) = \Delta_{\mathcal{M}_t} P(\mathbf{x}, t) \quad (2)$$

with initial condition $P(\mathbf{x}, 0) = Q(\mathbf{x})$. For each time t, $P(\mathbf{x}, t)$ represents a local mapping or equivalently coordinates associated to an evolving surface $\mathcal{M}_t$ whose $\Delta_{\mathcal{M}_t}$ is the Laplace-Beltrami operator and $H(\mathbf{x}, t)$ the mean-curvature. There are several numerical implementations of mean curvature flow using (normalized or not) umbrella operator [5] or finite element methods [3]. It is known that the mean curvature equation has a solution on a finite time interval and if $\mathcal{M}_0$ is convex it shrinks to a single point becoming asymptotically spherical [11]. It is also important to briefly recall that Laplace-Beltrami operator of a surface $\mathcal{M}$ is a functional $\Delta_{\mathcal{M}} : f \to \Delta_{\mathcal{M}} f$ that acts as a classical Laplacian (or second derivative) on a function $f : \mathcal{M} \to \mathbb{R}$. This operator has important spectral properties (see [17, 9]) since for the functional space of square integrable functions on $\mathcal{M}$ equipped with the scalar product $< f, g >= \int_{\mathcal{M}} fg$ there exists an orthonormal basis Φ_i and positive integers $0 = \lambda_0 < \lambda_1 \leq \lambda_2 \leq ... \leq \lambda_i$ such as $\Delta_{\mathcal{M}} \Phi_i = -\lambda_i \Phi_i$. Those manifold harmonics Φ_i represent brain shapes with slightly better sparsity than with spherical harmonics [17].

Last the volume inside the surface $\mathcal{M}$ can be efficiently computed by discretizing the following equality that is a consequence of Green-Ostrogradski formula:

$$\mathrm{Vol}(\mathcal{M}) = \int_{\mathcal{M}} F(\mathbf{x}) \cdot N(\mathbf{x}) d\mathbf{x} \quad (3)$$

provided that F is a vector field whose divergence is 1 (e.g. $F(x, y, z) = (x, 0, 0)$).

2.2 Mean curvature flow for retrospective morphogenesis

It has often been observed that mean curvature flow, Laplacian smoothing or truncation in manifold harmonics reconstruction are offering a striking analogy

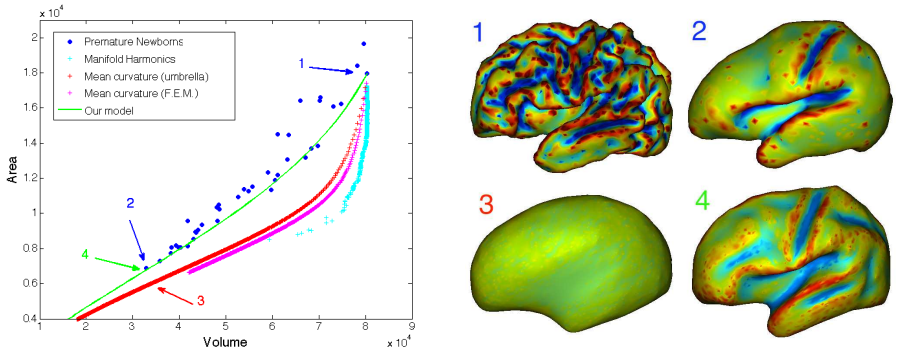

Fig. 1: Left: Trajectories in a Volume-Area plot with different techniques: mean curvature flow with two different discretization, manifold harmonics and our optimization method. Circles in blue correspond to Volume-Area measurements on Premature newborns. Right: Surfaces of premature newborns with largest (1) and smallest (2) volume. Mean-curvature flow (3) and our method (4) applied on surface (1) till reaching surface (2). Scales are not preserved for visualization. Only left hemispheres were considered.

with a developmental sequence of brains. This analogy can be illustrated by simple visualizations of real cortical surface versus smoothed ones or more objectively by comparing quantitative values such as volume or areas (see Fig. 1). In the case of mean curvature flow, the surface areas in the smoothed sequence are lower than expected from data. This supports that the shrinking process during smoothing is too fast and therefore we may compensate this effect by an "anti-shrinking" force, for instance proportional to $N(\mathbf{x}, t)$. When this proportionality factor equals the average of the mean curvature on $\mathcal{M}$, the volume is preserved [7] which is not the case in the developmental process. Thus we have adopted a pragmatic approach by adding a simple linear term $-aP(\mathbf{x}, t)$ to Eq. (1) and (2). In the case of a sphere this quantity has the same direction as the inward normal and one can consider that it is a crude approximation of normal direction for closed shapes. This leads to consider the following one-parameter model:

$$\partial_t P_a(\mathbf{x}, t) = \Delta_{\mathcal{M}_t} P_a(\mathbf{x}, t) - aP_a(\mathbf{x}, t) \tag{4}$$

This partial differential equation is non-linear and we can also propose a linear version by taking the laplacian $\Delta_{\mathcal{M}_0}$ on the original surface $\mathcal{M}_0$ instead of $\Delta_{\mathcal{M}_t}$. The following proposition will simplify optimization in the next part:

Proposition 1. *For each $a \in \mathbb{R}$, Eq. (4) and the equivalent with $\Delta_{\mathcal{M}_0}$ have an unique solution given by:*

$$P_a(\mathbf{x}, t) = e^{-at} P_0(\mathbf{x}, t) \tag{5}$$

Proof. Given the formula it is easy to compute $\partial_t P_a(\mathbf{x}, t)$ and to check that $P_a(\mathbf{x}, t)$ is solution of both PDE (4). We give in appendix a more constructive proof of this result in the linear case which involves Manifold Harmonics.

2.3 Parameter estimation

We consider a collection of surfaces $\mathcal{S} = \{S_1, ..., S_d\}$ that represents a reversed developmental sequence from a final surface S_1. Each surface S_i correspond to a gestational age (G.A.) t_i and $t_d \leq ... \leq t_1$. We have to define a criterion that measures the error between a real developmental sequence and a simulated one starting from a surface S_k with G.A. t_k through one of our two models. In the case of brain development, we only consider global quantities that are the volume ($\mathrm{Vol}(S)$) inside the surface and the total area ($\mathrm{Area}(S)$), respectively normalized by $\max_i \mathrm{Vol}(S_i)$ and $\max_i \mathrm{Area}(S_i)$. We can therefore define an error attached to a sequence $\mathcal{S}$, a starting surface S_k and a parameter a:

$$E(\mathcal{S}, t_k, a) = \sum_{i \leq k} d_i(a, t_i^*) \text{ with } t_i^* = \arg\min_t d_i(a, t) \tag{6}$$

where $d_i(a,t) = \Big[\mathrm{Area}(S_i) - \mathrm{Area}\big(P_a(\cdot, t)\big)\Big]^2 + \Big[\mathrm{Vol}(S_i) - \mathrm{Vol}\big(P_a(\cdot, t)\big)\Big]^2$. This error can be easily interpreted as the sum of distances between each data and the simulations $P_a(\cdot, t)$ obtained from S_k in a Volume-Area plot such as on Fig. 1. Our criterion to be minimized is defined in the Volume-Area space to avoid a direct identification of a simulation time t_i^* - that depends also on a - and a developmental time t_i.

Proposition 1 yields a trick to avoid a systematic computation of simulated surfaces for each value of a. Namely volumes and areas P_a are given by:

$$\mathrm{Vol}\big(P_a(\cdot,t)\big) = \mathrm{Vol}\big(P_0(\cdot,t)\big)e^{-3at},\ \mathrm{Area}\big(P_a(\cdot,t)\big) = \mathrm{Area}\big(P_0(\cdot,t)\big)e^{-2at} \quad (7)$$

since Eq. (5) can be simply understood as an homothety. To simplify notations we will denote them as $\mathrm{Vol}_a(t)$ and $\mathrm{Area}_a(t)$ in the following. Optimization of parameter a can then be done by using a classical low-dimensional approach such as Nelder-Mead Simplex Method.

When $a = 0$, we have classical formulas [7] that we will use at initial time

$$\frac{d\mathrm{Area}_0(t)}{dt} = -\int_{\mathcal{M}_t} H(\mathbf{x},t)^2 \qquad \frac{d\mathrm{Vol}_0(t)}{dt} = -\int_{\mathcal{M}_t} H(\mathbf{x},t) \quad (8)$$

Thus we can choose dt, discretization step of the mean curvature flow such as

$$A(S_k) - A_(S_{k-1}) \geq \alpha dt \widehat{H_k^2} \text{ and } V(S_k) - V(S_{k-1}) \geq \alpha dt \widehat{H_k} \quad (9)$$

for any starting surface S_k. The hat denotes an average of the mean curvature on the surface. For $\alpha = 10$ it guarantees to have a good sampling of the simulations in the Volume-Area domain. All the previous results can be summarized in:

Algorithm 1 Optimize Trajectory

Require: $\{S_1, ..., S_d\}$, $k \in \{1, .., d\}$

1: $\mathcal{M} := S_0$, i=0, Bool=TRUE
2: Compute biggest dt satisfying (9)
3: **while** Bool **do**
4: Compute A[i]:=Area($\mathcal{M}$) and Compute V[i]:=Vol($\mathcal{M}$) with Eq. (3)
5: Bool=A[i] > min Area(S_i) OR V[i] > min Vol(S_i)
6: Compute $\mathcal{M}$ at (i+1)dt with discretized Eq. (4)
7: i++
8: **end while**
9: Define objective function f($\cdot$)=$E(\mathcal{S}, t_k, \cdot)$ through Eq. (6) and (7)
10: a*=Nelder Mead Simplex Method (f)
11: **return** a*

3 Validation

3.1 Quantitative tools

Global geometric indices In a first attempt to validate our retrospective model we compared visual aspects of simulations to real data by using geometric measurements that can be done on the cortical surface. Rather than using directly principal curvatures we transformed these quantities in a more interpretable way thanks to *curvedness* and *shape index* (see [1] for a recent application in neuroimaging):

$$C(\mathbf{x}) = \sqrt{\kappa_1^2 + \kappa_2^2} \qquad SI(\mathbf{x}) = \frac{2}{\pi} \arctan \frac{\kappa_1 + \kappa_2}{\kappa_1 - \kappa_2} \tag{10}$$

Curvedness encodes the degree of folding whereas Shape Index that varies between -1 and +1 is scale invariant and only represents changes in local configurations at $\mathbf{x}$ from cusp (-1) to casp (1) through saddle (0) or cylinder (0.5). We compute three global indices ($\overline{C}$, $\overline{SI}_+$, $\overline{SI}_-$) from these two quantities by taking a) the median of $C(\mathbf{x})$, b) the median of $SI(\mathbf{x})$ for $\mathbf{x}$ such as $SI(\mathbf{x}) > 0$, c) the same for $SI(\mathbf{x}) < 0$.

Sulcus-based validation A second validation of our model was done by considering very early developing sulci such as the central one. Lines of central sulcus (CS) fundi were delineated semi-automatically [12]. Then evolution of these lines were followed through the developmental sequence and the simulations, provided that a matching process exists to register the surfaces. For a given surface $\mathcal{M}_t$ we defined the following mapping based on the three first manifold harmonics:

$$\mathbf{x} \to \Big(\Phi_1(\mathbf{x})^2 + \Phi_2(\mathbf{x})^2 + \Phi_3(\mathbf{x})^2\Big)^{-1/2} \Big(\Phi_1(\mathbf{x}), \Phi_2(\mathbf{x}), \Phi_3(\mathbf{x})\Big) \tag{11}$$

By construction it transforms each point of $\mathcal{M}_t$ to a point of the sphere of $\mathbb{R}^3$. Empirical properties of the 3 harmonics guarantee the transformation to be an homeomorphism, in particular the fact that $(\Phi_i)_{i=1,2,3}$ have always 2 nodal domains on the studied surfaces. If necessary we flip the sign of Φ_i by considering coordinates of their extremal points in a common 3D referential.

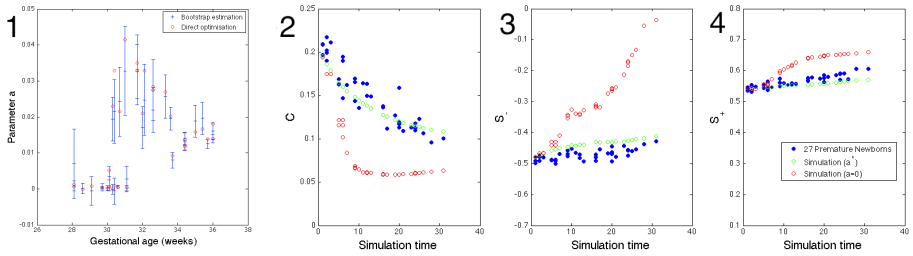

Fig. 2: 1: Sensibility analysis of parameter a for 35 largest brains: bootstrap estimation of mean and confidence intervals (blue) vs direct optimization (red). 2-4: Comparison of the three global indices ($\overline{C}$, $\overline{SI}_+$, $\overline{SI}_-$) between data (blue), our model (green) and mean curvature flow (red).

3.2 Results

Data We considered 40 T2-weighted images of preterm newborns with no apparent anatomical abnormalities and whose gestational age ranges from 26.7 to 35.7 weeks. They were segmented according to the method exposed in [6].

Sensibility analysis Our method allows a fast bootstrap estimation of the mean and confidence intervals of a_k^* (for the 35 largest brains to keep at least 5 points to estimate a) by applying algorithm (1) to different resampled sets $\{S_1^*, ..., S_d^*\}$ taken from $\mathcal{S}$ (45 s for 1000 bootstrapped samples). Comparison of a through direct optimization and through resampling is shown on Fig. 2 with respect to G.A. It seems that one can distinguish three different temporal periods ($28-31$, $31-34$, $34-36$) where the values of a are different as well as the sensibility.

Geometric measurements We compared the three global geometric indices between premature newborns, simulations with optimal parameter a^* and $a = 0$ starting from the largest brain S_1 (see Fig. 2). For each subject i we obtain a time t_i^* from Eq. (6) that can be located on the x-axis. The behavior of the different curves is reproducible with different initial brains S_k (not shown): one can observe that the median curvedness is decreasing from larger to smaller brains, whereas $\overline{SI}_+$ and $\overline{SI}_-$ are relatively more stable. It is quite remarkable to note the good fit of the optimal model and the divergence of mean curvature flow for

the three different measurements that are not surrogates of volume and areas.

Trajectory of central sulcus On Fig. 3 we have a direct comparison of the evolution of CS fundi on original surfaces and on corresponding smoothed surfaces with our model starting from the largest brain. The spherical mapping allows to see clearly a translation of CS lines when we start from older brains (yellow in the middle) to younger ones (black) and similarly from initial (yellow) to final (black) ones in the simulation.

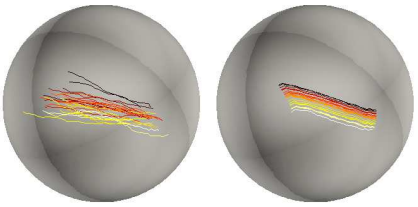

Fig. 3: Lines of CS fundi on real data (left) and on our simulations (right). See text for color code. North pole corresponds to frontal lobe.

4 Discussion

Our results demonstrate the feasibility of simulating the reversed cortical folding process observed on a cross-sectional study of premature newborns through a one parameter model derived from the mean curvature flow. Our model is only constrained by two global quantities, volume and area but it is able to predict evolution of geometrical quantities related to the shape of the cortical surfaces. Even if global, these quantities are not surrogates of those to optimize. More locally our model reproduces also a translation of central sulcus observed in the data that suggests a faster growth in frontal area than in parietal one that may be consistent with results in [15] for fetal brains from 24 to 28 G.A. Sensibility analysis on the parameter a reveals 3 different periods where its values and confidence intervals are fluctuating. Since a can be interpreted as the amplitude of an "anti-shrinking" force, this result suggests possible different scenarios in the cortical folding process with different kinetics. However larger confidence intervals in the interval $31 - 34$ G.A. may also come from a bias resulting from less time points to estimate the parameter.

In future works we intend to apply our method on fetal brains and compare their developmental trajectories to those of premature newborns such as in [4].

Longitudinal studies would also be an ideal application of our framework to compare more accurately in space the relevance of our model.

References

1. S. Awate, L. Win, P. Yushkevich, R. Schultz, and J. Gee. 3d cerebral cortical morphometry in autism: Increased folding in children and adolescents in frontal, parietal, and temporal lobes. *MICCAI 2008*, pages 559–567, 2008.
2. A. Cachia, J.F. Mangin, D. Riviere, F. Kherif, N. Boddaert, A. Andrade, D. Papadopoulos-Orfanos, J.B. Poline, I. Bloch, M. Zilbovicius, P. Sonigo, F. Brunelle, and J. Régis. A primal sketch of the cortex mean curvature: a morphogenesis based approach to study the variability of the folding patterns. *IEEE transactions on medical imaging*, 22(6):754–765, 2003.
3. U. Clarenz, U. Diewald, and M. Rumpf. Anisotropic geometric diffusion in surface processing. In *Proceedings of the conference on Visualization'00*, pages 397–405. IEEE Computer Society Press, 2000.
4. C. Clouchoux, D. Kudelski, A. Gholipour, S.K. Warfield, S. Viseur, M. Bouyssi-Kobar, J.L. Mari, A.C. Evans, A.J. du Plessis, and C. Limperopoulos. Quantitative in vivo mri measurement of cortical development in the fetus. *Brain Structure and Function*, 217(1):127–139, 2012.
5. M. Desbrun, M. Meyer, Schröder P., and A.H. Barr. Implicit fairing of irregular meshes using diffusion and curvature flow. In *Proceedings of the 26th annual conference on Computer graphics and interactive techniques*, pages 317–324, 1999.
6. J. Dubois, M. Benders, A. Cachia, F. Lazeyras, R. Ha-Vinh Leuchter, S.V. Sizonenko, C. Borradori-Tolsa, JF Mangin, and P.S. Hüppi. Mapping the early cortical folding process in the preterm newborn brain. *Cereb. Cort.*, 18(6):1444–1454, 2008.
7. J. Escher and G. Simonett. The volume preserving mean curvature flow near spheres. *Proceedings American Mathematical Society*, 126:2789–2796, 1998.
8. G. Geng, L.A. Johnston, E. Yan, J.M. Britto, D.W. Smith, D.W. Walker, and G.F. Egan. Biomechanisms for modelling cerebral cortical folding. *Medical Image Analysis*, 13(6):920–930, 2009.
9. D. Germanaud, J. Lefèvre, R. Toro, C. Fischer, J. Dubois, L. Hertz-Pannier, and J.-F. Mangin. Larger is twistier: Spectral analysis of gyrification (spangy) applied to adult brain size polymorphism. *NeuroImage*, 63(3):1257–1272, 2012.

10. N. Girard, C. Raybaud, and M. Poncet. In vivo mr study of brain maturation in normal fetuses. *American journal of neuroradiology*, 16(2):407–413, 1995.
11. Gerhard Huisken. Flow by mean curvature of convex surfaces into spheres. *Journal of Differential Geometry*, 20(1):237–266, 1984.
12. A Le Troter, D Rivière, and O Coulon. An interactive sulcal fundi editor in brainvisa. In *17th International Conference on Human Brain Mapping, Organization for Human Brain Mapping*, 2011.
13. J. Lefèvre and J.F. Mangin. A reaction-diffusion model of human brain development. *PLoS computational biology*, 6(4):e1000749, 2010.
14. J. Nie, L. Guo, G. Li, C. Faraco, L.S. Miller, and T. Liu. A computational model of cerebral cortex folding. *Journal of theoretical biology*, 264(2):467–478, 2010.
15. V. Rajagopalan, J. Scott, P.A. Habas, K. Kim, J. Corbett-Detig, F. Rousseau, A.J. Barkovich, O.A. Glenn, and C. Studholme. Local tissue growth patterns underlying normal fetal human brain gyrification quantified in utero. *The Journal of Neuroscience*, 31(8):2878–2887, 2011.
16. J.A. Scott, P.A. Habas, V. Rajagopalan, K. Kim, A.J. Barkovich, O.A. Glenn, and C. Studholme. Volumetric and surface-based 3d mri analyses of fetal isolated mild ventriculomegaly. *Brain Structure and Function*, pages 645–655, 2012.
17. S. Seo and M.K. Chung. Laplace-beltrami eigenfunction expansion of cortical manifolds. In *IEEE International Symposium on Biomedical Imaging*, 2011.
18. D.A. Striegel and M.K. Hurdal. Chemically Based Mathematical Model for Development of Cerebral Cortical Folding Patterns. *PLoS Comput Biol*, 5(9), 2009.
19. R. Toro. On the possible shapes of the brain. *Evol. Biol.*, 39(4):600–612, 2012.
20. P. Yu, P.E. Grant, Y. Qi, X. Han, F. Ségonne, R. Pienaar, E. Busa, J. Pacheco, N. Makris, R.L. Buckner, et al. Cortical surface shape analysis based on spherical wavelets. *Medical Imaging, IEEE Transactions on*, 26(4):582–597, 2007.

Appendix: proof of Proposition 1

We decompose $P_a(\mathbf{x}, t)$ in the basis of eigenfunctions of the operator $\Delta_{\mathcal{M}_0}$:

$$P_a(\mathbf{x}, t) = \sum_{i=0}^{+\infty} \hat{\mathbf{p}}_i(a, t)\Phi_i(\mathbf{x})$$

where $\hat{\mathbf{p}}_i(a,t) \in \mathbb{R}^3$ is given by $\int_{\mathcal{M}_0} P_a(\mathbf{x},t)\Phi_i(\mathbf{x})d\mathbf{x}$. Then since P_a satisfies Eq. (4) (with $\Delta_{\mathcal{M}_0}$ instead of $\Delta_{\mathcal{M}_t}$):

$$0 = \partial_t P_a - a\Delta_{\mathcal{M}_0} P_a + aP_a = \sum_{i=0}^{+\infty} \Big[\partial_t \hat{\mathbf{p}}_i(a,t) + \lambda_i \hat{\mathbf{p}}_i(a,t) + a\hat{\mathbf{p}}_i(a,t)\Big]\Phi_i(\mathbf{x})$$

So $\hat{\mathbf{p}}_i(a,t) = \hat{\mathbf{p}}_i(a,0)e^{-\lambda_i t}e^{-at}$. Last we have to notice that $\hat{\mathbf{p}}_i(a,0)$ is independent of a since they correspond to the coefficients of the initial surface $\mathcal{M}_0$ and that $\hat{\mathbf{p}}_i(a,0)e^{-\lambda_i t}$ are the coefficients of $\mathcal{M}_t$ for $a = 0$. We conclude that $P_a(\mathbf{x},t) = e^{-at}P_0(\mathbf{x},t)$.